SSRG International Journal of Electrical and Electronics Engineering
ISSN: 2348-8379/ https://doi.org/10.14445/23488379/IJEEE-V13I9P111

Volume 13 Issue 9, 136-147, September 2026

Original Article

Illuminance Evaluation in Urban Roadways using UAV and IoT for Dark Zone Detection and Public Lighting Inspection

Jhonny Roy Condori Cahuaya[1], Bryan Gomez Pacheco[2], Jezzy James Huaman Rojas[3]

[1,2,3]*School of Electrical Engineering, Universidad Continental, Huancayo, Peru.*

[3]*Corresponding Author : jhuamanroj@continental.edu.pe*

Received: 20 August 2026 Revised: 11 September 2026 Accepted: 15 September 2026 Published: 26 September 2026

Abstract - *Conventional public lighting inspections have difficulty capturing illumination reductions in certain areas, as they only cover a specific geographical location. This study develops and tests a UAV-IoT system to analyze the distribution of illumination from LED lighting within three urban districts. The proposed system combines equipment that includes a BH1750 sensor and an ESP32-C3 microcontroller, along with UAV data collection and transmission of the data to an IoT system. The campaign included 90 spatial positions distributed between roadway and sidewalk areas, three runs per segment, and 20,250 samples acquired at a nominal height of 0.5 m. The lowest levels were consistently located around longitudinal position X_3, with minimum values at X_3-Y_3 for both evaluated surfaces. T_2 had the highest average illuminance, whereas T_3 had the lowest. Comparison with a reference lux meter at 24 spatial positions yielded a MAPE of 0.183%, an RMSE of 0.245 lux, and an R^2 of 0.99998. IoT communication showed an overall packet loss of 0.69%. The system provides a multipoint representation of the illuminance distribution and enables the location of sectors requiring subsequent photometric verification.*

Keywords - *LED public lighting, Illuminance, Internet of Things, Unmanned Aerial Vehicle, Low-illuminance zones.*

1. Introduction

Public lighting is an infrastructure linked to nighttime mobility, the visibility of pedestrians and drivers, and the perception of safety in urban spaces. Available evidence indicates that lighting interventions can be associated with changes in certain safety indicators and that the characteristics of the luminous environment also influence users' perception of risk [1, 2]. Consequently, the evaluation of an installation should not be limited to verifying whether luminaires are operational, but should also consider how lighting is distributed over surfaces intended for vehicular and pedestrian traffic.

The incorporation of LED luminaires and Internet of Things (IoT) technologies has expanded the possibilities for monitoring urban lighting. The review presented in [3] shows that smart lighting systems have evolved toward architectures with distributed sensors, network communications, remote control, and energy management.

However, a significant proportion of these developments is oriented toward switching, power regulation, energy consumption, and luminaire maintenance, whereas the spatial characterization of illuminance on the service surface receives less attention.

From a photometric point of view, the functioning of luminaires cannot guarantee uniform illuminance distribution along a road. Study [4] explores the uniformity of pedestrian lighting and indicates that spatial factors due to the geometry of the installation and distribution of light are among the factors that influence pedestrian lighting uniformity. Thus, measurements performed only in the vicinity of luminaires may not represent the intermediate or lateral sectors where lighting is reduced. This factor gains importance when the road and the adjacent sidewalk are in different positions with regard to the light sources.

The limitations of the operation and the constraints of the measurements that can be made manually led to the development of mobile platforms to extend the area that can be inspected. Study [5] made in situ measurements of road lighting using an instrumented vehicle and showed the possibility of at least partly automating the measurement process. Studies [6, 7] used measurement campaigns to analyze the photometric performance of LED systems and adaptive lighting in real operating conditions. These measurements show that it is necessary to increase both the number and the spatial continuity of measurements. While the use of land platforms has improved over the years, it is still constrained by the trajectory that the platform is able to cover.

The photometric measurement of defined areas can be accomplished by using Uncrewed Aerial Vehicles (UAVs). Study [8] integrated a UAV, a BH1750 sensor, positioning, and remote transmission, and used digital processing for the measurement of road illuminance. It has also been documented that, from nighttime measurements of the lighted environment, drones can carry photometric sensors. Study [10] focused on the use of UAVs for photometric measurement and argued the importance of orienting, positioning, and controlling the measurement geometry.

In public lighting, IoT applications have focused on monitoring and controlling the infrastructure. One example is study [11], which built a monitoring and control system with LoRa, whereas study [12] integrated IoT-based technologies for lighting control within a smart city framework. At a higher city-based perspective, study [13] analyzed different public lighting improvements and their relationships to various types of crime and incivilities. However, study [13] did not analyze the spatial distribution of the lighting along the road. Study [14] was one of the first to consider the integration of EdgeML into a smart lighting system.

In spite of this work, there is still a gap in the integration of systems designed to control the luminaires, take mobile measurements, and carry out joint spatial inspections of both the vehicular and pedestrian surfaces. Existing studies demonstrate the feasibility of using mobile sensors and UAVs to measure photometric variables. Still, there is limited experimental evidence for schemes that combine a multipoint grid for roadway and sidewalk measurements, repeated routes, platform-stability control, IoT transmission, and instrumental comparison within a single campaign.

This study develops and evaluates a UAV-IoT system to characterize the spatial distribution of illuminance on urban roads with LED public lighting. The platform integrates a BH1750 sensor, an ESP32-C3 microcontroller, UAV-based acquisition, and communication with an IoT infrastructure. The experimental strategy separates roadway and sidewalk using a longitudinal and transverse grid, repeats measurements across three routes, and preserves information on flight stability to identify records affected by wind or tilt. The evaluation is complemented by a reference lux meter to quantify the correspondence between both systems.

The objective was to implement and evaluate the UAV-IoT platform to identify spatial variations and sectors with lower illuminance within three urban road segments. The system is proposed as a complementary tool for identifying sectors that require subsequent photometric evaluation, rather than as a substitute for normative procedures. The rest of the article presents the platform and experimental procedure, followed by spatial illuminance analysis, comparison with the reference lux meter, IoT communication performance, and acquisition stability. Subsequently, the results are compared with previous studies, and the system's scope and main limitations are defined.

2. Materials and Methods

2.1. Study Area and Experimental Design

The experimental campaign was conducted across three segments of an urban road network with LED public lighting. The sectors were identified as T_1, T_2, and T_3. T_1 corresponds to Av. Primero de Mayo, between Jr. Las Praderas and Av. Huancavelica; T_2 comprises the Jr. Los Ángeles–Jr. Los Manzanos sector, between Av. Primero de Mayo and Av. Mariátegui and T_3 corresponds to the Jr. Magdalena–Jr. Yapallana sector, between Av. Primero de Mayo y Jr. Los Manzanos.

The location of the segments and the distribution of the measurement points are presented in Figure 1. The study area map was represented in the WGS84/UTM zone 18S system. The location of each measurement within the segment was managed using a local coordinate system associated with the experimental grid.

Fig. 1 Study area and spatial distribution of the segments and measurement points considered in the illuminance evaluation using the UAV-IoT system

Each segment was divided into five longitudinal positions, X_1–X_5, corresponding to 10%, 30%, 50%, 70%, and 90% of its length. For each longitudinal position, three transverse positions were established on the roadway and three on the sidewalk. This configuration produced 15 positions per surface and 30 positions per segment. The measurements were repeated through three independent runs, R_1, R_2, and R_3. In total, 90 spatial positions were evaluated, and 270-point records were generated.

2.2. UAV-IoT Measurement Platform

The acquisition platform consisted of a UAV, a BH1750 digital illuminance sensor, an ESP32-C3 microcontroller, and a web infrastructure for supervision and record storage. The sensor module was installed on the UAV structure in a fixed arrangement relative to the aircraft. Figure 2 presents the platform used during the campaign and the mounting of the measurement module.

Fig. 2 UAV-IoT platform used for illuminance measurement: (a) UAV with the installed sensor module, (b) Detail of the BH1750 mounting, and (c) and (d) System deployment during the nighttime campaign.

Each record stored the segment, run, point code, surface, longitudinal and transverse positions, local coordinates, height, illuminance, UAV orientation (roll and pitch), battery level, record status, and operational incidence.

2.3. Spatial Sampling Scheme on Roadway and Sidewalk

A localized x-, y-, and z-coordinate system was used to define the spatial distribution. The x-axis represented the longitudinal displacement of the segment. The y-axis was used to define transverse displacement, and the z-axis was used to define the height of the sensor. In T_1, the longitudinal positions were 3.0, 9.0, 15.0, 21.0, and 27.0 m; in T_2, 3.2, 9.6, 16.0, 22.4, and 28.8 m; and in T_3, 2.8, 8.4, 14.0, 19.6, and 25.2 m. The transverse roadway positions were −2.10, 0, and 2.10 m in T_1; −2.16, 0, and 2.16 m in T_2; and −2.04, 0, and 2.04 m in T_3. For the sidewalk, 3.90, 4.50, and 5.10 m were used for T_1; 3.96, 4.50, and 5.04 m for T_2; and 3.84, 4.50, and 5.16 m for T_3. The grid geometry is presented in Figure 3.

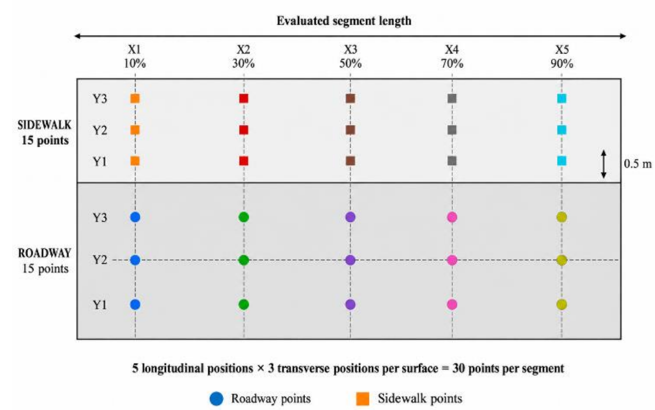

Fig. 3 Spatial grid scheme for measuring illuminance on roadway and sidewalk using five longitudinal positions (X_1–X_5) and three transverse positions (Y_1–Y_3) on each surface

2.4. Illuminance Acquisition Procedure

Measurements were taken at grid positions in the defined order. During the measurements, the UAV was held at 0.5 meters above the measurement surface. Each of the positions was measured in runs R_1, R_2, and R_3. Each position contained a record of 75 samples at a nominal interval of 200 ms, which corresponds to a sampling frequency of 5 Hz and a nominal window of 15 seconds. Each run contained 2250 samples, each segment 6750 samples, and the complete campaign 20,250 samples. The general configuration is summarized in Table 1.

Table 1. Experimental configuration for illuminance acquisition using the UAV-IoT system

Parameter	Configuration
Evaluated segments	3 (T_1, T_2, and T_3)
Evaluated surfaces	Roadway and sidewalk
Points per segment	30
Roadway points per segment	15
Sidewalk points per segment	15
Runs per segment	3 (R_1, R_2, and R_3)
Nominal sensor height	0.5 m
Acquisition duration per point	15 s
Nominal interval between samples	200 ms
Nominal sampling frequency	5 Hz
Samples per point	75
Point records	270
Total samples	20 250

The data acquisition system collects and stores the original reading from the sensor identified as $E_{raw\_BH1750\_lux}$ and the variable E_{corr_lux}, which will be used in the data processing and analysis. Both variables are stored separately in the acquisition database.

2.5. Web platform and IoT Data Management

A web platform was developed to control and monitor the test, and for measurement data logging and visualization in a time series. Each test could be identified, and the duration and sampling of the test and the generation of CSV files for the subsequent test data processing procedure could be defined. During each test, a local log of sensor data was maintained, and information was transmitted through the IoT infrastructure. For each segment of the track and each test, 2250 local logs were maintained, corresponding to the 30 evaluated points with 75 samples per point. In the IoT infrastructure, the system considered 450 expected messages for each test, the actual number of messages, the percentage of lost messages, the average latency, maximum latency, mean Received Signal Strength Indicator (RSSI), number of disconnections, and the battery level at the start and end of the run. The splitting of light measurement data and communication data allowed the measurement system to be assessed in operation and to evaluate the data transmission system. Illuminance data gave insights on the spatial light distribution. Operational data of the communication system were evaluated. The web platform allowed control of the tests, storage, and data retrieval for each of the tests conducted during the campaign. In addition, the web platform allowed the visualization of temporal data acquisition, including the samples for each test. Figure 4 shows the web interface for each test control and data storage and retrieval for each of the campaign tests.

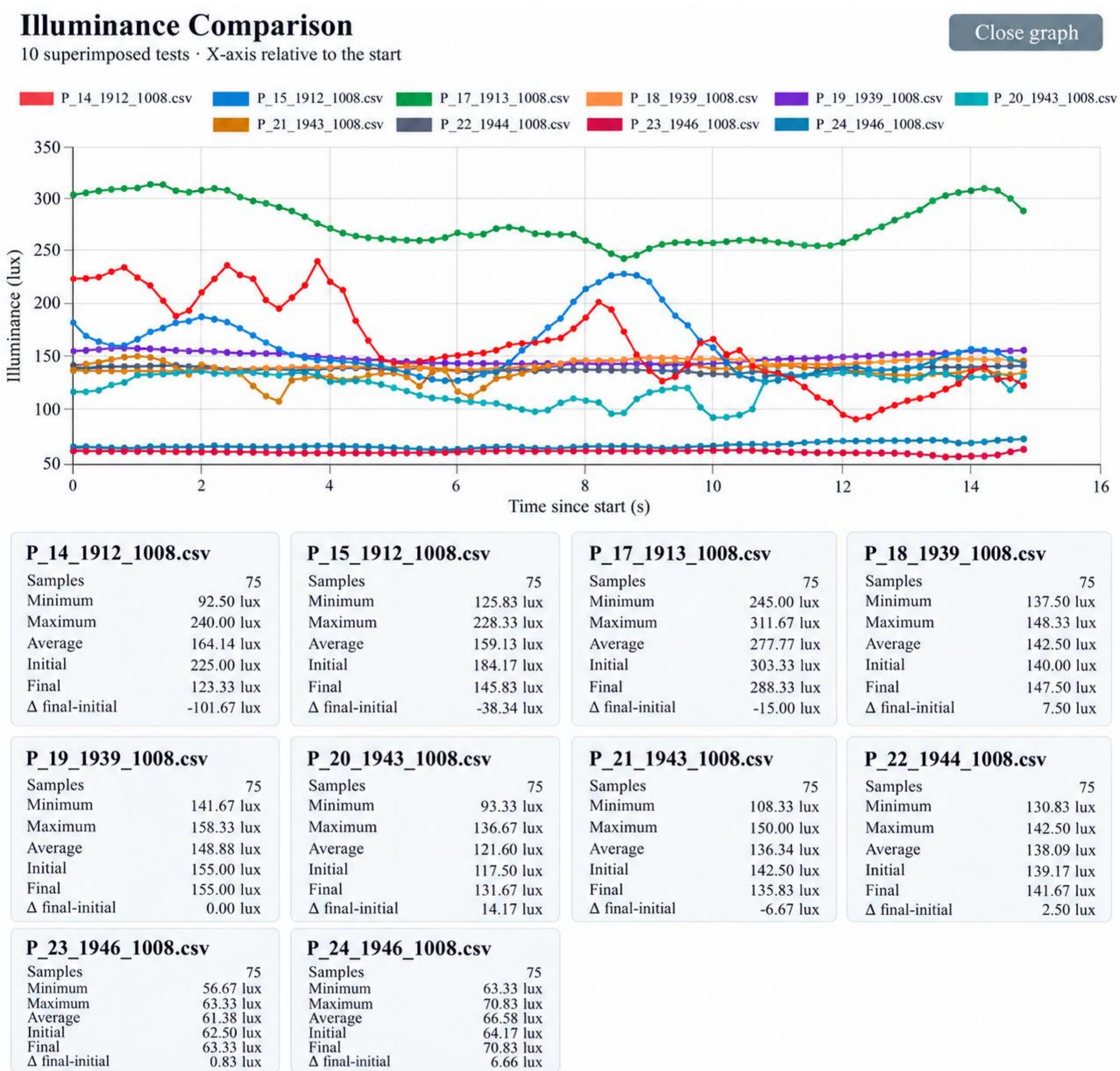

Fig. 4 Web platform used for test control, record storage, and temporal visualization of illuminance measurements from the UAV-IoT system

2.6. Stability Control and Measurement Quality

Illuminance acquisition using an aerial platform may be affected by variations in position and orientation during flight. For this reason, quality control considered both the photometric signal and the variables associated with UAV behavior. For each sample, roll and pitch angles, measurement height, record status, and the presence of incidences during acquisition were recorded.

Records obtained under the expected operating conditions were classified as valid. When disturbances associated with wind or UAV tilt were identified during acquisition, the corresponding record was marked for review using the WIND/TILT incidence.

The WIND/TILT classification was used as an operational criterion recorded during the campaign. No numerical threshold for roll, pitch, or coefficient of variation was established to perform this classification automatically. Records identified with this incidence were retained in the database to preserve measurement traceability and to analyze their temporal behavior subsequently. To characterize the variation of each record, the standard deviation, coefficient of variation, illuminance range, and sample evolution during the acquisition window were considered. The temporal behavior of the records allows observation of differences between a stable acquisition and one affected by wind or tilt conditions. Figure 5 presents an example of both cases during the measurement window.

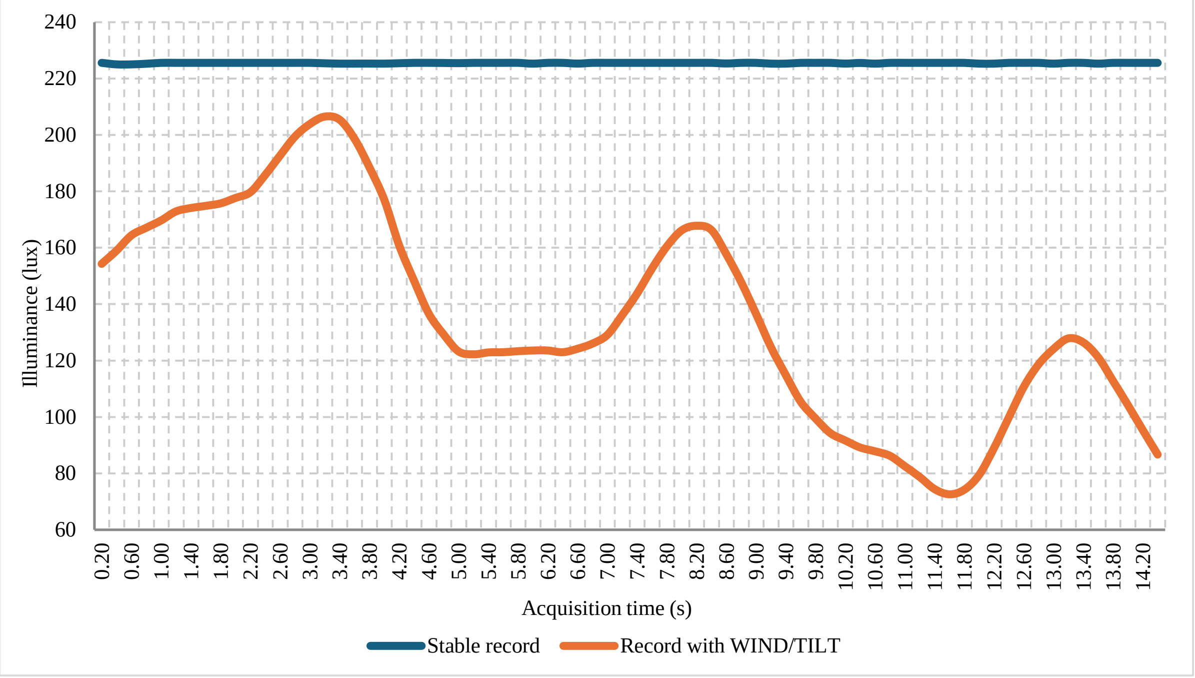

Fig. 5 Temporal behavior of a stable record and of a record affected by wind/tilt during illuminance acquisition with the UAV-IoT system

2.7. Comparison with the Reference Lux Meter

The response of the UAV-IoT system was compared with a reference lux meter. The validation was performed at 24 spatial positions, eight per segment, distributed between four roadway positions and four sidewalk positions. At each selected position, three consecutive readings were taken with the lux meter. These readings were averaged to obtain a single representative reference value for each position.

The resulting value was compared with the average illuminance recorded by the UAV-IoT system during run R_2 at the same position. Thus, the instrumental comparison was performed using 24 spatial pairs, eight corresponding to each segment. For each position, the difference between the average obtained with the UAV-IoT system and the mean value of the three lux meter readings was determined. The correspondence between the two systems was characterized using the Mean Absolute Error (MAE), Root Mean Square Error (RMSE), Mean Absolute Percentage Error (MAPE), and the coefficient of determination (R^2). A relative error criterion of ±1% was used for the comparison. This percentage corresponds only to the criterion used to evaluate the difference between both systems and does not represent the specified accuracy of the lux meter.

2.8. Data Processing and Analysis

The records were organized by segment, run, evaluated surface, longitudinal position *X*, and transverse position *Y*. For each point, the 75 samples acquired during the nominal measurement window were processed. The photometric analysis was performed using the variable E_{corr_lux}, corresponding to the value recorded in the acquisition database for measurement processing.

The average illuminance of each record was calculated as follows:

$$E_{prom} = \frac{1}{n}\sum_{i=1}^{n} E_i \quad (1)$$

Where E_i corresponds to each illuminance sample and n = 75.

The temporal variability of each record was characterized using the coefficient of variation:

$$CV = \frac{SD}{E_{prom}} \cdot 100 \quad (2)$$

Where SD represents the standard deviation of the 75 samples.

To standardize the time axis of the stability representations, elapsed time was defined from the sample index and the nominal acquisition interval of 0.2 s:

$$t_i = (i-1) \cdot 0.2 \quad (3)$$

Where i represents the sample number. Thus, the 75 values for each record ranged from 0 to 14.8 s.

The spatial analysis was performed independently for the roadway and sidewalk. For each combination of segment, surface, position *X*, and position *Y*, a representative value was calculated by averaging the E_{prom} values corresponding to the available runs classified as valid for that position. These values were then used to obtain descriptive statistics by segment and surface and to construct longitudinal profiles and two-dimensional illuminance representations.

The sectors with lower illuminance were identified descriptively based on the spatial minima observed within each grid and their recurrence among runs. In this study, the term dark zone is used operationally to refer to a sector that presents a local illuminance minimum relative to the evaluated grid; it does not represent a classification of regulatory non-compliance based on an absolute threshold. Records identified with WIND/TILT incidence were retained for stability and traceability analysis, but they were not used as primary observations in the spatial reconstruction.

For the comparison with the reference lux meter, the difference between both readings was defined as:

$$e_i = E_{UAV,i} - E_{ref,i} \quad (4)$$

Where $E_{UAV,i}$ corresponds to the average illuminance obtained using the UAV-IoT system and $E_{ref,i}$ to the average of the three lux meter readings at position *i*.

The mean absolute error was calculated as:

$$MAE = \frac{1}{N}\sum_{i=1}^{N}\left|E_{UAV,i} - E_{ref,i}\right| \quad (5)$$

The root mean square error was obtained as:

$$RMSE = \sqrt{\frac{1}{N}\sum_{i=1}^{N}(E_{UAV,i} - E_{ref,i})^2} \quad (6)$$

and the mean absolute percentage error as:

$$MAPE = \frac{100}{N}\sum_{i=1}^{N}\left|\frac{E_{UAV,i}-E_{ref,i}}{E_{ref,i}}\right| \quad (7)$$

where N = 24 corresponds to the number of positions used in the instrumental comparison. For each position, $E_{ref,i}$ represents the average of the three consecutive readings obtained with the lux meter, and $E_{UAV,i}$ corresponds to the average illuminance recorded by the UAV-IoT system during R_2 at the same position. Communication variables were analyzed independently of the photometric variables. For each run, the expected and received messages, packet loss, average and maximum latency, average RSSI, and number of disconnections were considered.

3. Results

3.1. Illuminance Distribution by Segment and Surface

The spatial analysis was performed using records classified as valid while keeping roadway and sidewalk measurements separate.

For each grid position, a representative value was obtained from the available runs, and the descriptive statistics were subsequently calculated by segment and surface. The results are summarized in Table 2.

Table 2. Descriptive statistics of illuminance by segment and evaluated surface

Segment	Surface	Valid positions	E_{prom} (lux)	E_{min} (lux)	E_{max} (lux)	Spatial SD (lux)
T_1	Roadway	15	160.61	59.57	269.23	60.04
T_1	Sidewalk	14	80.86	13.47	152.76	41.57
T_2	Roadway	15	178.28	65.97	312.65	67.80
T_2	Sidewalk	15	98.06	14.98	174.70	50.36
T_3	Roadway	15	123.53	31.46	220.71	52.00
T_3	Sidewalk	15	65.23	6.97	116.75	37.05

T_2 presented the highest average illuminance values, with 178.28 lux on the roadway and 98.06 lux on the sidewalk. T_1 recorded intermediate values of 160.61 and 80.86 lux, respectively, whereas T_3 presented the lowest averages, with 123.53 lux on the roadway and 65.23 lux on the sidewalk. In the three segments, the average recorded on the sidewalk was lower than that corresponding to the roadway.

The relative difference between both surfaces was 49.7% in T_1, 45.0% in T_2, and 47.2% in T_3. The longitudinal distribution also showed differences between positions. On the roadway, X_3 recorded averages of 84.19 lux in T_1, 91.00 lux in T_2, and 47.88 lux in T_3. On the sidewalk, the corresponding values were 36.50, 41.31, and 24.88 lux. The complete profiles for the five longitudinal positions are presented in Figure 6.

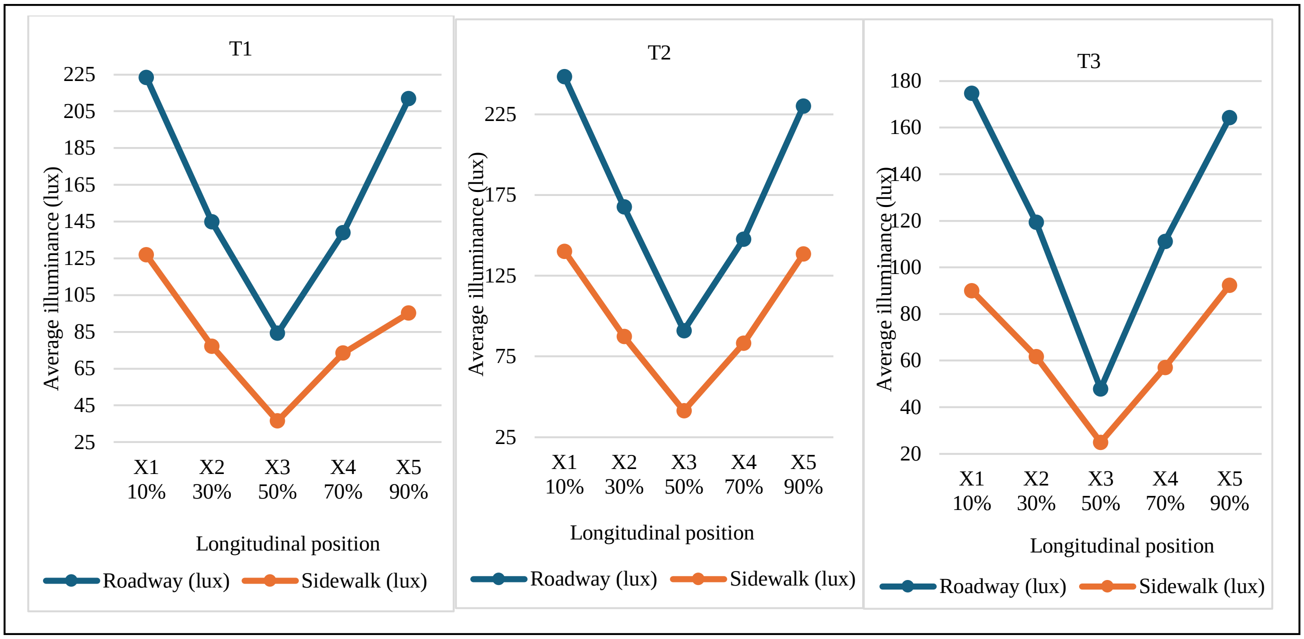

Fig. 6 Longitudinal profiles of average illuminance on the roadway and sidewalk for segments T_1, T_2, and T_3

In T_1, one sidewalk position was not included in the spatial analysis because the three available records for that position were classified as WIND/TILT incidence.

The remaining segment-surface combinations retained the 15 planned positions.

3.2. Identification of Sectors with Lower Illuminance

Comparing representative values within each grid enabled locating positions with lower illuminance. In the six segment-surface combinations, the minimum value was recorded at X_3-Y_3. Table 3 presents these minima and their differences relative to the point of highest illuminance on the same surface.

Table 3. Positions with lower illuminance identified in each segment and surface

Segment	Surface	Minimum position	Local E_{min} (lux)	Maximum position	Local E_{max} (lux)	Reduction (%)
T_1	Roadway	X_3-Y_3	59.57	X_1-Y_2	269.23	77.88
T_1	Sidewalk	X_3-Y_3	13.47	X_1-Y_1	152.76	91.18
T_2	Roadway	X_3-Y_3	65.97	X_1-Y_2	312.65	78.90
T_2	Sidewalk	X_3-Y_3	14.98	X_5-Y_1	174.70	91.42
T_3	Roadway	X_3-Y_3	31.46	X_1-Y_2	220.71	85.75
T_3	Sidewalk	X_3-Y_3	6.97	X_5-Y_1	116.75	94.03

On the roadway, the reduction between the minimum and maximum of each segment was 77.88% in T_1, 78.90% in T_2, and 85.75% in T_3. On the sidewalk, the reductions were 91.18, 91.42, and 94.03%, respectively. T_3 presented the lowest minimum values of the campaign: 31.46 lux on the roadway and 6.97 lux on the sidewalk.

At longitudinal position X_3 of this segment, the representative roadway values were 35.25 lux at Y_1, 76.93 lux at Y_2, and 31.46 lux at Y_3; on the sidewalk, the values were 40.53, 27.15, and 6.97 lux, respectively. The two-dimensional distribution of the representative values for the three segments is presented in Figure 7.

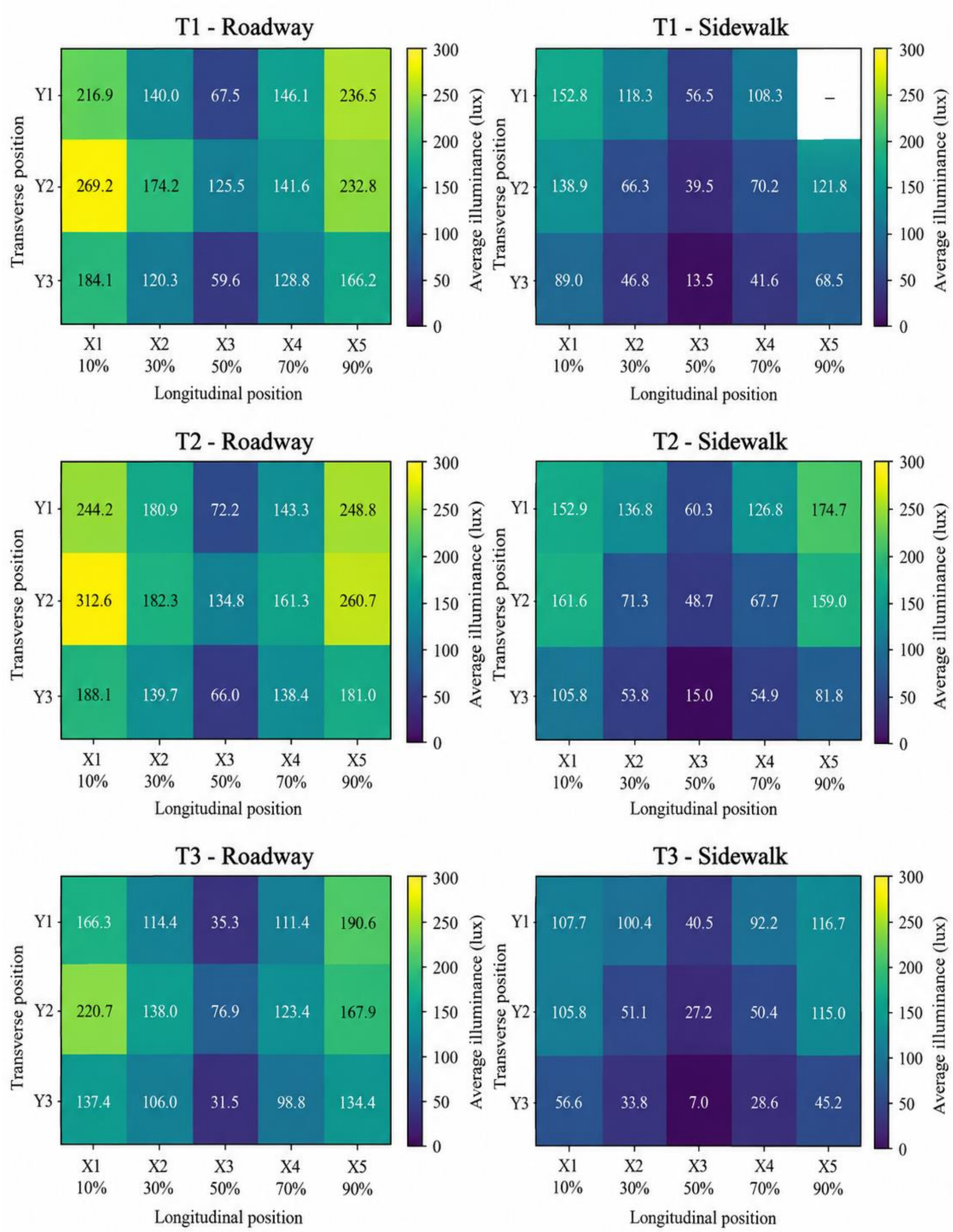

Fig. 7 Spatial distribution of average illuminance in the roadway and sidewalk grids of segments T_1, T_2, and T_3. Values correspond to the average of the runs classified as valid

3.3. Comparison with the Reference Lux Meter

The instrumental comparison comprised 24 spatial positions distributed across the three segments. For each position, the average of the three consecutive lux meter readings was calculated, and the resulting value was compared with the average illuminance recorded by the UAV-IoT system during R_2 at the same position. For the complete dataset, an MAE of 0.195 lux, an RMSE of 0.245 lux, a MAPE of 0.183%, and a coefficient of determination $R^2 = 0.99998$ were obtained. The indicators obtained for each segment are presented in Table 4.

T_2 presented the highest MAE, with 0.285 lux, whereas T_3 recorded the lowest, with 0.081 lux. The MAPE remained below 0.30% in the three segments.

The greatest absolute difference between the compared mean values was 0.511 lux, and the highest absolute relative error was 0.638%. Consequently, the 24 spatial pairs remained within the ±1% criterion used for the comparison. The relationship between the values obtained using both systems is presented in Figure 8.

Table 4. Comparison of indicators between the UAV-IoT system and the reference lux meter

Segment	*N*	MAE (lux)	RMSE (lux)	MAPE (%)	R^2
T_1	8	0.218	0.265	0.183	0.99998
T_2	8	0.285	0.313	0.272	0.99997
T_3	8	0.081	0.106	0.094	0.99999
Total	24	0.195	0.245	0.183	0.99998

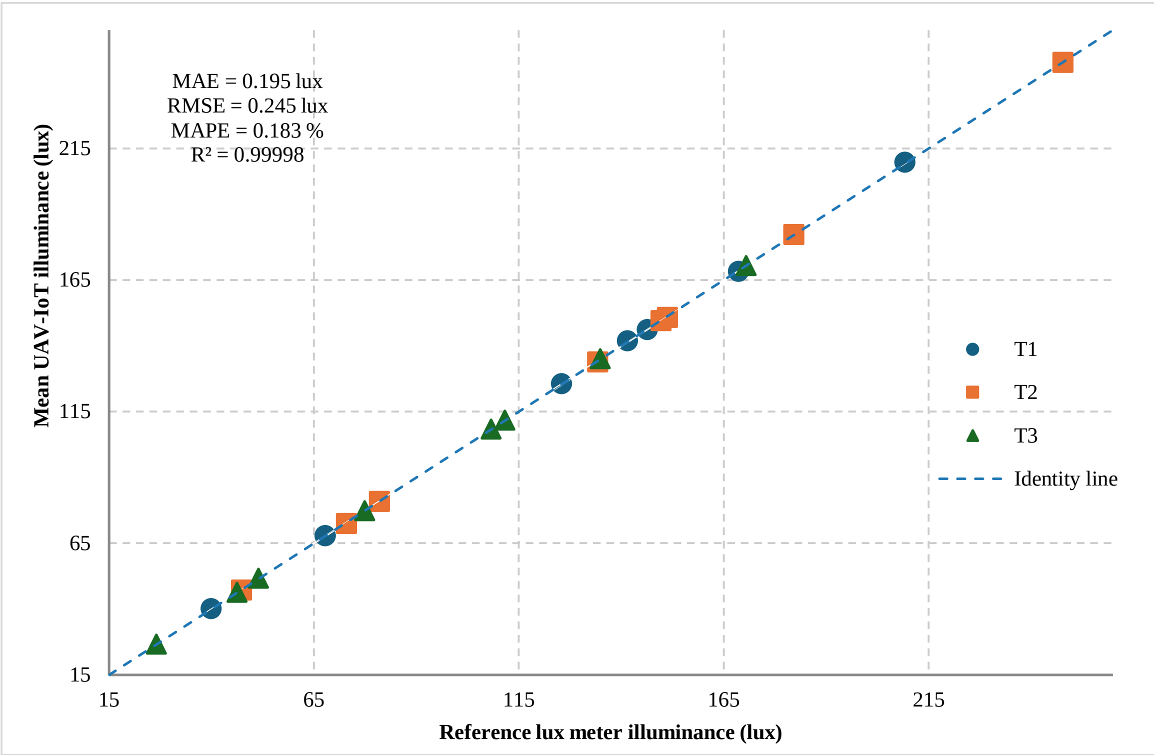

Fig. 8 UAV-IoT and reference lux meter comparison at 24 validation points

3.4. Operational Performance of IoT Communication

Communication performance was evaluated over the nine runs. In each run, 450 IoT messages were expected, representing 1350 messages per segment and 4050 messages for the entire campaign. A total of 1335 messages were received in T_1, 1345 in T_2, and 1342 in T_3. The consolidated indicators by segment are presented in Table 5.

For the set of nine runs, 4022 of the 4050 expected messages were received, equivalent to an overall packet loss of 0.69%. The overall average latency was 0.181 s, and the maximum recorded latency was 0.548 s. Four disconnections were counted: two in T_1, two in T_2, and none in T_3. Local storage retained 2250 illuminance samples per run, regardless of the number of messages received via the IoT link.

Table 5. IoT communication performance indicators by segment

Segment	Expected messages	Received messages	Packet loss (%)	Average latency (s)	Maximum latency (s)	Average RSSI (dBm)	Disconnections
T_1	1350	1335	1.11	0.174	0.458	−64.49	2
T_2	1350	1345	0.37	0.205	0.548	−58.23	2
T_3	1350	1342	0.59	0.165	0.512	−64.64	0

3.5. Acquisition Stability and Quality Control

Quality control identified 15 records with WIND/TILT incidence among the 270 records obtained during the campaign, equivalent to 5.56% of the total. The remaining 255 records, corresponding to 94.44%, were classified as valid for the main spatial analysis.The distribution of incidences was not uniform across surfaces. In T_1, six records were identified for review, two on the roadway and four on the sidewalk; in T_2, four were recorded, one on the roadway and three on the sidewalk; and in T_3, five were identified, two on the roadway and three on the sidewalk. Table 6 summarizes the distribution of these records.

Table 6. Distribution of records identified with WIND/TILT incidence

Segment	Surface	Total records	WIND/TILT records	Incidence (%)
T_1	Roadway	45	2	4.44
T_1	Sidewalk	45	4	8.89
T_2	Roadway	45	1	2.22
T_2	Sidewalk	45	3	6.67
T_3	Roadway	45	2	4.44
T_3	Sidewalk	45	3	6.67
Total	**Roadway + sidewalk**	**270**	**15**	**5.56**

Ten of the 15 records identified with WIND/TILT corresponded to the sidewalk and five to the roadway. The highest proportion occurred on the T_1 sidewalk, with four records out of 45, equivalent to 8.89%. Records associated with WIND/TILT did not show a single magnitude of temporal variation. The T_3-R_1-R-X_2-Y_2 record presented a CV of 27.95% and a range of 134.17 lux, whereas other records with the same incidence showed considerably smaller ranges. The temporal contrast between a stable acquisition and one affected by wind or tilt was previously presented in Figure 5 of the quality control procedure.

4. Discussion

The spatial evaluation showed that the roadway and sidewalk do not present the same illuminance distribution within the analyzed segments. The lower levels recurrently recorded on the sidewalks indicate that an inspection focused only on the vehicular surface may provide an incomplete characterization of lighting conditions. Study [4] indicates that pedestrian lighting uniformity depends on the installation's geometric and photometric configuration. Complementarily, studies [15, 16] address the lighting of pedestrian spaces from the perspectives of uniformity and luminous-environment quality, respectively.

These precedents support the convenience of treating the roadway and sidewalk as distinct surfaces, although the perceptual variables considered in [15, 16] were not examined in the present work. The recurrence of the lowest levels around X_3 among the valid runs indicates that the pattern was not restricted to a single acquisition. This condition is consistent with the principle of increasing the spatial density of measurements used in mobile inspection platforms. Study [5] used an instrumented vehicle to perform in situ road lighting measurements, whereas studies [17, 18] developed mobile systems to increase coverage and associate measurements with their positions. Compared with these terrestrial approaches, the platform used in this research enabled the application of the same sampling structure on the roadway and sidewalk, as well as the repetition of positions across different runs.

Among the reviewed studies, [8] presents a configuration similar to that developed in this research, integrating a UAV with a BH1750 sensor for measuring road illuminance. In its multipoint evaluation, a MAPE of 5.08% was reported, whereas in the present campaign, a MAPE of 0.183% was obtained relative to the reference lux meter. This numerical difference does not constitute evidence of the proposed system's superiority, since the scenarios, reference instruments, acquisition geometries, and processing procedures were not equivalent. The comparison only makes it possible to situate the observed behavior with respect to a methodologically close precedent.

The instrumental comparison also yielded an RMSE of 0.245 lux and an R^2 of 0.99998 across the 24 evaluated positions. At each position, the reference value corresponded to the average of three consecutive lux meter readings. The proximity of the values resulting from both systems also supports the use of the platform to spatially discriminate zones with diverse illuminance levels in the given conditions. Nevertheless, a high coefficient of determination in the relationship between the two series indicates metrological equivalence, and in the absence of it, the indicators need to be considered in the range and configuration of the experiment.

The WIND/TILT incidence records show that there must be consideration of the platform stability during the acquisition. Operational classification allowed retaining these records for traceability and, in the meantime, eliminated them from the main spatial analysis. The variability among records of the same incidence indicates that WIND/TILT cannot be interpreted only in terms of the coefficient of variation of illuminance.

Studies [9, 10] indicate that, when performing photometric measurements using UAVs, the geometry and stability of the platform need to be considered. Therefore, it is necessary to carry out a subsequent study in order to quantify the relation of photometric error and the degree of roll and pitch, in order to establish automatic acceptance criteria.

The spatial minima around X_3 cannot be attributed to a single factor. Study [19] demonstrates that barriers can affect the lighting on a road, and study [20] shows that the geometry and the characteristics of the installation can affect its photometric behavior. In this work, luminaire spacing, photometric curves, the height of the installation, and potential obstructions were not studied in a systematic manner.

Therefore, the minima found need to be interpreted as illuminance gaps, and the possible causes need to be investigated later in order to draw a conclusion.

The architecture of the implemented IoT system is unlike many of the smart lighting systems described in the literature. In [11, 12], communication and IoT technologies were used for measuring, monitoring, and controlling the lighting infrastructure. In the evaluated platform, the IoT link did not control luminaires. Rather, the aerial capture link and IoT were used for record supervision and data transfer. Sample preservation at the local site avoided the loss of photometric information when communication was lost due to occasional communication failures.

The spatial identification of sectors with lower illuminance may help prioritize points for subsequent inspection. Still, these results do not permit conclusions about urban safety. Study [13] found associations between public lighting interventions and changes in certain crimes and incivilities; however, the present research did not evaluate crime, perceived safety, pedestrian behavior, or user visibility. Consequently, the scope of the results remains limited to photometric and spatial characterization.

The results of the research can only be extended within the boundaries of the experimental parameters. This particular case was a three-segmented urban campaign, a measurement height of 0.5 m, and a particular combination of UAV, sensor, and specific acquisition method. In this research, other heights, different types of roads, and dissimilar environmental conditions were not analyzed. Therefore, the results of this research cannot be generalized, and the data cannot be used to describe the compliance status. This research attempts to bring together multiple activities previously done independently, such as multiple aerial acquisitions, separate analyses of the roadway and the sidewalk, repeated runs, and operational stability. The combination of these activities allows the construction of a representation of illuminance and helps in determining zones that presumably have undue concentration. Additionally, the data can be used as a starting point to develop an automated system to detect abnormal cases. Study [14] focuses on smart lighting systems and supports that the use of EdgeML, along with a distributed architecture, will start to provide intelligence at the edge to systems. These functionalities were neither implemented nor assessed on the current platform.

5. Conclusion

Using a UAV-IoT system, illuminance characterization on roadways and sidewalks was achieved with a longitudinal multipoint grid. The distribution provided an intermediate location for lower-illuminance sections and distinguished between the behavior of surfaces used by vehicles and pedestrians. When compared to a lux meter, used at 24 spatial points, a MAPE of 0.183%, RMSE of 0.245 lux, and R^2 = 0.99998 were achieved. The photometric records were preserved due to local storage and IoT communication, even when the transmission was lost.

The purpose of the system is to complement other tools to increase inspection coverage and identify regions that need further photometric examination. The system is limited by the 0.5 m nominal measurement height, the platform's stability, and the characteristics of the three sections. As such, the results cannot confirm compliance with regulations. The next stage will focus on incorporating additional road configurations to better validate the system.

Conflicts of Interest

The authors declare that there is no conflict of interest regarding the publication of this paper.

Funding Statement

The authors received no specific funding for this research.

Acknowledgments

The authors thank the academic and technical support provided during the development of this research.

References

[1] Brandon C. Welsh, David P. Farrington, and Stephen Douglas, "The Impact and Policy Relevance of Street Lighting for Crime Prevention: A Systematic Review based on a Half-Century of Evaluation Research," *Criminology and Public Policy*, vol. 21, no. 3, pp. 739-765, 2022. [CrossRef] [Google Scholar] [Publisher Link]

[2] Dongpil Son et al., "Street Lighting Environment and Fear of Crime: A Simulated Virtual Reality Experiment," *Virtual Reality*, vol. 29, no. 1, pp. 1-17, 2025. [CrossRef] [Google Scholar] [Publisher Link]

[3] Siwar Khemakhem, and Lotfi Krichen, "A Comprehensive Survey on an IoT-based Smart Public Street Lighting System Application for Smart Cities," *Franklin Open*, vol. 8, 2024. [CrossRef] [Google Scholar] [Publisher Link]

[4] Constantinos A. Bouroussis, and Annika K. Jägerbrand, "Simulations and Analysis of the Optimum Uniformity for Pedestrian Road Lighting Focusing on Energy Performance and Spill Light in the Roadside Environment," *Energies*, vol. 15, no. 9, pp. 1-21, 2022. [CrossRef] [Google Scholar] [Publisher Link]

[5] Cheng-Hsien Chen et al., "Design of an Equipped Vehicle for in Situ Road Lighting Measurement," *Sustainability*, vol. 15, no. 13, pp. 1-15, 2023. [CrossRef] [Google Scholar] [Publisher Link]

[6] Lodovica Valetti et al., "Long-Term Monitoring Campaign of LED Street Lighting Systems: Focus on Photometric Performances, Maintenance and Energy Savings," *Sustainability*, vol. 15, no. 24, pp. 1-32, 2023. [CrossRef] [Google Scholar] [Publisher Link]

[7] Gianni Pasolini et al., "Comprehensive Assessment of Context-Adaptive Street Lighting: Technical Aspects, Economic Insights, and Measurements from Large-Scale, Long-Term Implementations," *Sensors*, vol. 24, no. 18, pp. 1-25, 2024. [CrossRef] [Google Scholar] [Publisher Link]

[8] Songhai Xu et al., "Design and Application Research of a UAV-based Road Illuminance Measurement System," *Automation*, vol. 5, no. 3, pp. 407-431, 2024. [CrossRef] [Google Scholar] [Publisher Link]

[9] Katarzyna Bobkowska et al., "An Innovative New Approach to Light Pollution Measurement by Drone," *Drones*, vol. 8, no. 9, pp. 1-19, 2024. [CrossRef] [Google Scholar] [Publisher Link]

[10] Bertalan Pizág, Dániel Kacz, and Balázs Vince Nagy, "A Drone-based Photometric Measurement Platform," *Journal of Field Robotics*, vol. 39, no. 8, pp. 1218-1230, 2022. [CrossRef] [Google Scholar] [Publisher Link]

[11] F. Sánchez Sutil, and Antonio Cano-Ortega, "Smart Public Lighting Control and Measurement System using Lora Network," *Electronics*, vol. 9, no. 1, pp. 1-28, 2020. [CrossRef] [Google Scholar] [Publisher Link]

[12] Pathomthat Chiradeja, and Suntiti Yoomak, "Development of Public Lighting System with Smart Lighting Control Systems and Internet of Things (IoT) Technologies for Smart City," *Energy Reports*, vol. 10, pp. 3355-3372, 2023. [CrossRef] [Google Scholar] [Publisher Link]

[13] Pablo Cadena-Urzúa, Javier Guardiola, and Francisco Montes, "The Impact of Public Lighting Improvement on Crimes and Incivilities Reduction in Chile," *Frontiers in Sociology*, vol. 10, pp. 1-7, 2025. [CrossRef] [Google Scholar] [Publisher Link]

[14] Gaetanino Paolone et al., "Smart Lighting Systems: State-of-the-Art in the Adoption of the Edgeml Computing Paradigm," *Future Internet*, vol. 17, no. 2, pp. 1-50, 2025. [CrossRef] [Google Scholar] [Publisher Link]

[15] Ulrika Wänström Lindh, and Annika K. Jägerbrand, "Perceived Lighting Uniformity on Pedestrian Roads: From an Architectural Perspective," *Energies*, vol. 14, no. 12, pp. 1-20, 2021. [CrossRef] [Google Scholar] [Publisher Link]

[16] Ming Liu et al., "Evaluating Street Lighting Quality in Residential Areas by Combining Remote Sensing Tools and a Survey on Pedestrians' Perceptions of Safety and Visual Comfort," *Remote Sensing*, vol. 14, no. 4, pp. 1-25, 2022. [CrossRef] [Google Scholar] [Publisher Link]

[17] Piotr Tomczuk et al., "Evaluation of Street Lighting Efficiency using a Mobile Measurement System," *Energies*, vol. 14, no. 13, pp. 1-25, 2021. [CrossRef] [Google Scholar] [Publisher Link]

[18] Piotr Jaskowski, Piotr Tomczuk, and Marcin Chrzanowicz, "Construction of a Measurement System with GPS RTK for Operational Control of Street Lighting," *Energies*, vol. 15, no. 23, pp. 1-22, 2022. [CrossRef] [Google Scholar] [Publisher Link]

[19] Jingzhi Ren et al., "Analysis of Light Obstruction from Street Lighting in Road Scenes," *Remote Sensing*, vol. 15, no. 24, pp. 1-20, 2023. [CrossRef] [Google Scholar] [Publisher Link]

[20] Krzysztof Zima, and Wojciech Ciepłucha, "Efficiency Analysis of Roadway Lighting Replacement in a Selected Polish Municipality," *Applied Sciences*, vol. 13, no. 5, pp. 1-17, 2023. [CrossRef] [Google Scholar] [Publisher Link]